RSC Advances

PAPER

View Article Online
View Journal | View Issue

Cite this: *RSC Adv.*, 2022, **12**, 9917

Toward layered MoS_2 anode for harvesting superior lithium storage†

Ying Zhang, [ab] Hanisha Ponnuru,[ab] Qinting Jiang,[ab] Hui Shan,[ab] Hirbod Maleki Kheimeh Sari, [ab] Wenbin Li,[ab] Jingjing Wang,[ab] Junhua Hu, [c] Jianhong Peng*[d] and Xifei Li *[ab]

As a typical transition metal dichalcogenide (TMD), molybdenum disulphide (MoS_2) has become one of the most promising anode materials for lithium-ion batteries (LIBs) due to its desirable electrochemical properties. But the development of commercial MoS_2 is limited by the problem of agglomeration. Thus, the production of MoS_2 nanosheets with few (<10) layers is highly desired but remains a great challenge. In this work, a facile and scalable approach is developed to prepare large-flake, few-layer (4–8) MoS_2 nanosheets with the assistance of ultrasonics. Simultaneously, the as-prepared MoS_2 nanosheets and commercial bulk MoS_2 were analysed under multiple spectroscopic techniques and a series of electrochemical tests to understand the dependence of electrochemical performance on structural properties. When used as anode materials for LIBs, the obtained MoS_2 nanosheets provide a reversible capacity of 716 mA h g^{-1} at 100 mA g^{-1} after 285 cycles, and demonstrated an excellent capacity retention rate of up to 80%. Compared with that of commercial MoS_2 (14.8%), the capacity retention rate of our MoS_2 nanosheets has a significant improvement. This work explored the ability of few-layered MoS_2 nanosheets in the field of LIBs while suggesting the commercialization of the MoS_2 by an ultrasonicated ball milling exfoliation technique.

Received 10th November 2021
Accepted 7th March 2022

DOI: 10.1039/d1ra08255h

rsc.li/rsc-advances

Introduction

Lithium-ion batteries (LIBs) have become the most indispensable item of supreme energy storage that is prospering in electronic devices and automobile industries. Accompanying the people's continuing demand for high energy and power densities and a keen motive to lower the environmental impact, the components and commercialization of LIBs have turned out to be a topic of extensive scientific research for a couple of decades.[1–3] Of late, numerous LIB anode materials, ranging from carbonaceous material like graphite to transition metal-based two-dimensional materials (TMDs) like molybdenum disulphide (MoS_2), molybdenum selenide ($MoSe_2$), molybdenum trioxide (MoO_3) and tungsten disulphide (WS_2), are being investigated due to their exceptional crystal structures that contribute to remarkable electrochemical, electrical and optical properties.[4–7] As conventional graphite anodes produced a considerably lower theoretical capacity of 372 mA h g^{-1}, the latest TMDs have portrayed a higher capacity of over 500 mA h g^{-1} exceeding those of the bulk equivalents.[7–9]

MoS_2 has been verified as one of the most assuring anode materials by exhibiting a theoretical capacity of over 669 mA h g^{-1} with a low reaction potential.[10] These unique properties could potentially be applicable in fields such as capacitors, lubricants, catalysts and even as an extraordinary anode material for LIBs.[11–16] The morphology of MoS_2 nanosheets comprises covalently bonded sulphur–molybdenum–sulphur atoms which are weakly stacked by van der Waals forces in order to form layers of two dimensions.[9,17–21] The interaction of these layers enables the lithium ions to diffuse between the layers through intercalation without an obvious expansion in volume.[16,22,23] These reported insights of MoS_2 have aided us to understand the influence of morphology on electrochemical properties, the intercalation capacity of lithium, and the lithiation and delithiation cycle of LIB.[24,25]

Furthermore, a minimal layering of MoS_2 nanosheets has demonstrated an extended reversibility capacity while supporting a faster Li ion intercalation process compared with that of bulk MoS_2. This excellent storage response with a negligible Li ion diffusion limit is due to the surface area offered by

[a]*Xi'an Key Laboratory of New Energy Materials and Devices, Institute of Advanced Electrochemical Energy, School of Materials Science and Engineering, Xi'an University of Technology, Xi'an, Shaanxi, 710048, China. E-mail: xfli2011@hotmail.com*

[b]*Shaanxi International Joint Research Center of Surface Technology for Energy Storage Materials, Xi'an, Shaanxi, 710048, China*

[c]*Center for International Cooperation on Designer Low-carbon & Environmental Materials (CDLCEM), Zhengzhou University, Zhengzhou, Henan, 450001, China*

[d]*School of Physical and Electronic Information Engineering, Qinghai Nationalities University, Xining, China. E-mail: pjhhj@sohu.com*

† Electronic supplementary information (ESI) available. See DOI: 10.1039/d1ra08255h

nanosheets of fewer than 10 layers with adequate interlayer and interplanar spacing.[26] Nevertheless, agglomeration of the nanosheets has been shown to compromise the electrochemical performance of the cell in numerous cases.[27–33] Thus, an effective synthesis is essential for fabricating high performance MoS_2 anodes.

There are various bottom-up[34] and top-down[35] approaches to produce MoS_2 but attaining a few layers of nanosheets continued to be a massive challenge through the years.[26] Generally, the bottom-up approach requires an extreme energy intensive post-treatment under stringent conditions, making it a least preferred process.[36,37] In spite of low yields, the top-down approach is commonly preferred on account of the bulk material abundance.[38] Liquid phase exfoliation (LPH), mechanical exfoliation (ME), ball milling (BM) and alkali-ion intercalation (AII) are a few processes chosen to create desirable layers, but there are advantages and disadvantages associated with these techniques in terms of process conditions and quality of nanosheets.[39–49] Of all the mentioned techniques, ball milling was recognized as the most scalable and commercialized method of nanosheet production.[49,50] However, the pure ball milling method cannot give full play to the advantages of the layered structure of MoS_2.[51] Additionally, ball milling has the ease of coupling with numerous auxiliary methods to obtain nanostructure-like sheets and flakes of the desired dimensions and composition by altering the process conditions.[2,26,50,52,53] Therefore, we proposed ultrasonic-assisted ball milling. The preparation method reduces the size of MoS_2 by ball milling on the one hand, and obtains few-layer MoS_2 by ultrasonic peeling on the other hand. The corresponding discussion is later in the paper.

Therefore, this paper aims to report the potential of minimal-layered MoS_2 nanosheets, fabricated from a simple ultrasonicated ball milling exfoliation method, over commercial bulk MoS_2. The as-prepared MoS_2 material was demonstrated to be composed of only 4–8 layers and investigated under multiple spectroscopic techniques to understand the structural and morphological properties in comparison with those of commercial bulk MoS_2. Benefiting from the non-agglomerated lamella structure, the electrochemical performance of the MoS_2 anode is significantly improved by the controllable exfoliation of MoS_2 compared with that of commercial MoS_2. Besides, the mechanism involved in the synthesis of MoS_2 nanosheets is illustrated to show the impact of the selected approach on structural properties and the ease of fabrication. Collectively, this provides an effective strategy for the exfoliation of other bulk materials, which has great significance for future material design and applications in energy conversion and storage devices.

Experimental

Exfoliation of MoS_2

Firstly, 500 mg of commercial bulk MoS_2 with a 325 mesh was dispersed in 5 mL of anhydrous ethanol solvent. The mixture was ball-milled continuously for 12 h at a speed of 450 rpm on a planetary mill with zirconia grinding balls and vials. The obtained dispersion was then ultrasonicated at ambient temperature for 5 h to produce a colloidal suspension of MoS_2 nanosheets. The suspension was subjected to centrifugation at 5000 rpm for 15 min to remove any large particles, including partially exfoliated bulk MoS_2 and unexfoliated residual bulk MoS_2.

Fabrication of MoS_2 anode electrode

According to previous reports,[27] a vacuum filtration method was employed to obtain the MoS_2 nanosheet anode on Celgard 2400 as a LIB polypropylene separator. Following the mentioned procedure, the as-prepared suspension was filtered through a porous filter paper, Celgard 2400 polypropylene separator, forming the MoS_2 film. Subsequently, the film was dried in a vacuum chamber at 80 °C for 72 h, and the MoS_2 anode electrode was obtained. In parallel, for comparison, the commercial MoS_2 anode electrode was prepared by slurry-casting on Cu foils that served as current collectors. The slurry contained 80 wt% bulk MoS_2, 10 wt% carbon black (CB) and 10 wt% poly(vinylidene) fluoride (PVDF) binder in a *N*-methylpyrrolidinone (NMP) solvent. The obtained electrode was dried in a vacuum at 90 °C overnight. The electrodes were then subjected to material characterization techniques.

Material characterization

The morphology of the bulk and prepared MoS_2 was analysed in a field emission scanning electron microscope (FE-SEM, Hitachi S-4800), transmission electron microscope (TEM, Hitachi H-7000), and high-resolution transmission electron microscope (HRTEM, JEOL 2010F). The powder X-ray diffraction (XRD) pattern was recorded by a Rigaku RU-200BVH diffractometer using a Co-Kα source ($\lambda = 1.7892$ Å).

Electrochemical measurements

Coin-type electrochemical half-cells were used; the working electrode was the prepared anode electrode and the counter electrode was a lithium foil. The electrolyte for the system consisted of 1 M $LiPF_6$ salt dissolved in ethylene carbonate (EC) : diethyl carbonate (DEC) : ethyl methyl carbonate (EMC) with a volume ratio of 1 : 1 : 1. The CR-2032 button battery was assembled in a dry glove box filled with argon (moisture and oxygen concentration < 1 ppm). A Princeton ParSTAT MC 2000A was utilized to perform cyclic voltammetry (CV) at a potential of 0.01 to 3.0 V (*vs.* Li/Li^+) at a scan rate of 0.1 mV s^{-1}. The charging and discharging characteristics were tested using a Neware CT-4000 battery tester at room temperature and constant current between 0.01 and 3.0 V (*vs.* Li/Li^+).

Results and discussion

Fig. 1a shows the XRD patterns of bulk and as-prepared MoS_2 as black and blue lines, respectively. The typical diffraction peaks of the bulk MoS_2 finely matched the standard peaks of the hexagonal phase (JCPDS 37-1492). The as-prepared MoS_2 sample represented five peaks corresponding to the (002), (004), (103), (006) and (008) planes in which a sharp peak is clear for

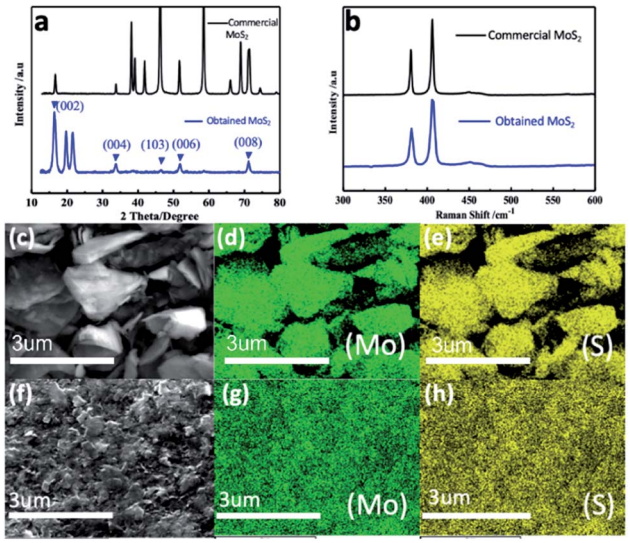

Fig. 1 (a) XRD patterns and (b) Raman spectra of commercial MoS_2 (black line) and obtained MoS_2 (blue line) nanosheets; SEM element mappings of (c–e) commercial MoS_2 and (f–h) MoS_2 nanosheets: (d and g) are of Mo and (e and h) are of S.

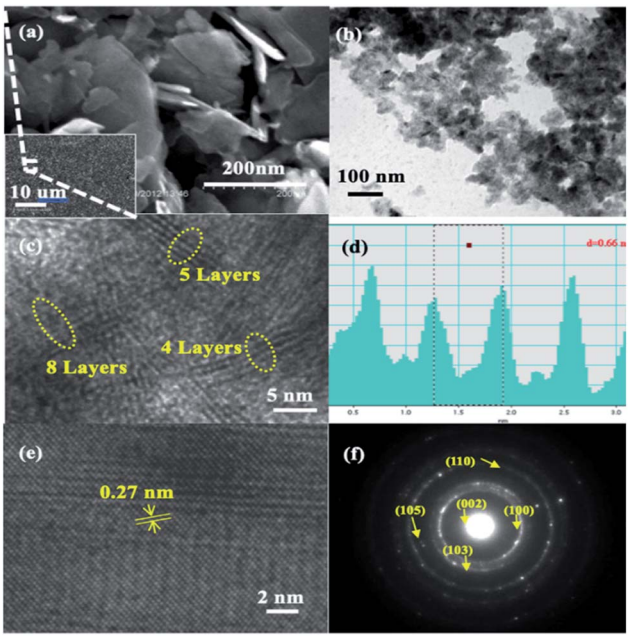

Fig. 2 MoS_2 nanosheets: (a) SEM and (b) TEM images; (c) lateral view of the MoS_2 layers measured by HRTEM; (d) intensity profile along the MoS_2 layers in (c) with nm units for the *x*-axis; (e) HRTEM image of a MoS_2 nanosheet for interplanar spacing; (f) SAED pattern of a MoS_2 nanosheet.

(002) and confirms the well-stacked layered structure formation.[21,54–56] Additionally, the larger peak widths clearly convey that the obtained MoS_2 has a smaller particle size compared with that of bulk MoS_2.[57]

Raman spectra of the bulk and as-prepared MoS_2 are compared in Fig. 1b, in which the spectra show the same set of peaks. The two typical Raman active modes located at 380 cm^{-1} and 406 cm^{-1} can be attributed to E^1_{2g} and A_{1g}, resulting from the inlayer vibration of molybdenum and sulphur atoms along with the vibration of sulphides in the out-of-plane direction.[58–61] Furthermore, Fig. 1c–h depict the elemental mappings of the bulk and as-prepared MoS_2, where Fig. 1c and f are the overall images of the bulk and as-prepared MoS_2. In the following images, it is worth noting that the atoms of Mo and S are evenly distributed in the two samples. The energy dispersive X-ray spectroscopy (EDX) associated with the functioning of HRTEM (Fig. S1†) shows that the as-prepared MoS_2 consists only of Mo and S, which further confirms the Mo : S atomic ratio of 1 : 2; as agreed with the elemental composition of MoS_2.

Moreover, SEM was employed to observe the morphology of the bulk MoS_2 (shown in Fig. S2†). The random-shaped MoS_2 displayed a sheet-like morphology with a thickness of *ca.* 1 μm. The as-prepared MoS_2, as shown in Fig. 2a, exhibits a different morphology from that of the bulk one (Fig. S2†) signifying the essence of ball milling that decreased the size of MoS_2 nanosheets dramatically. Similarly, the TEM image of the as-prepared MoS_2 in Fig. 2b confirms the presence of thin MoS_2 nanosheets. HRTEM (Fig. 2c) showcases the lateral view of a few lamellar structures with visible lattice fringes. Evidently, each film is composed of 4–8 MoS_2 layers, that is, significantly reduced compared with those in the bulk MoS_2 structure or any MoS_2 nanosheet structures reported earlier. A characteristic peak that belongs to the [002] direction of the MoS_2 nanosheets is demonstrated in Fig. 2d. The interlayer spacing is measured to be ~0.66 nm and is consistent with the (002) plane of a layered hexagonal MoS_2. This result reveals that each molybdenum atom layer is sandwiched between two sulphur atom layers. In addition to the interlayer spacing, the HRTEM image in Fig. 2e clearly illustrates the lattice fringes of MoS_2 nanosheets with an elaborative crystal structure, in which the interplanar distances were measured to be 0.27 nm, corresponding to the (100) plane of MoS_2.[47,62] The several bright rings in Fig. 2f, as shown by Selected Area Electron Diffraction (SAED), coincide with the hexagonal MoS_2 structure's diffraction pattern by further indicating the good stacking of MoS_2 nanosheets with different crystallographic orientations.[63,64] Additionally, the diffraction dots within the diffraction rings were identified as (002), (100), (103), (105), and (110) planes, which confirms the high crystallinity of the MoS_2 nanosheets.[65]

Through the above material characterization techniques and analysis, it can be deduced that the observations that emerged from the exfoliated MoS_2 nanosheets *via* ultrasonic assisted ball milling process are admirable and satisfactory for commercial usage in LIBs. The desirable structural characteristics are possible due to the approach proposed and employed in this study to synthesize MoS_2 nanosheets (as displayed in Fig. 3). After stage I, the layered MoS_2 was dispersed into ethanol and ball-milled for 12 h. That the shear force from ball milling is superior to that of the weak van der Waals interactions between the MoS_2 layers resulted in the easy exfoliation of some MoS_2 layers during the process of ball milling.[66] In the case of unexfoliated MoS_2, the ethanol solvent intercalated between the MoS_2 layers, resulting in an increased layer distance. The

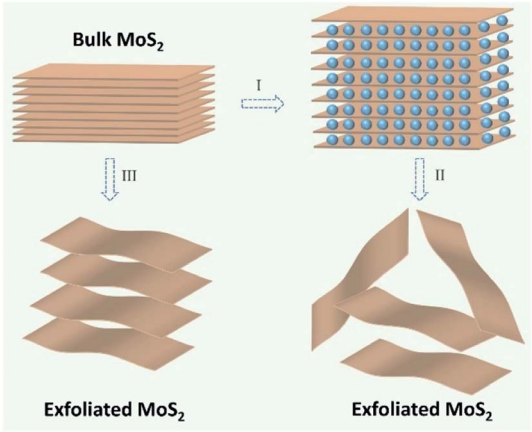

Fig. 3 Schematic illustration for MoS_2 nanosheet synthesis: (I) ball milling; (II) ultrasonic exfoliation; (III) untreated.

exfoliation of MoS_2 inevitably occurred when ultrasonics was employed (stage II). However, commercial MoS_2 layers were stacked together *via* relatively weak van der Waals interactions, as represented in stage III.

Lithium storage properties of bulk and as-prepared MoS_2 were studied by a series of electrochemical tests, such as cyclic voltammetry (CV) and galvanostatic charge–discharge (GCD) testing. Fig. 4 shows the voltage range from 0.01 V to 3.00 V. First, the CV of bulk MoS_2 and the prepared MoS_2 under a scan rate of 0.1 mV s^{-1} were evaluated. The CV curves of the two samples were performed and evaluated as for the first scan. Firstly, in the first cathodic scan,[67–70] the two peaks at 0.89 and 1.08 V correspond to the insertion of Li^+ with the formation of Li_xMoS_2 ($MoS_2 + xLi^+ + xe^- = Li_xMoS_2$) for the bulk and as-prepared MoS_2, respectively. Inclusively, another obvious reduction peak (positioned at 0.35 and 0.52 V for bulk and as-prepared MoS_2, respectively) indicates the existence of an electrochemical reduction that originates from a conversion reaction ($Li_xMoS_2 + 4Li^+ + 4e^- = 2Li_2S + Mo/Li_y$), in which the formation of Mo metal along with the Li_2S from Li_xMoS_2 occurs. In the opposite process (anodic scan), one obvious oxidation peak due to the oxidation of Li_2S into sulphur shows a similar reaction potential at ~2.30 V for two anodes.[70,71] If a comparative analysis is carried out of the second and third CV curves of bulk MoS_2, a big difference can be observed, which reveals a poor cyclic performance. In the case of the as-prepared MoS_2, these two CV curves nearly overlap, verifying superior cyclic performances.

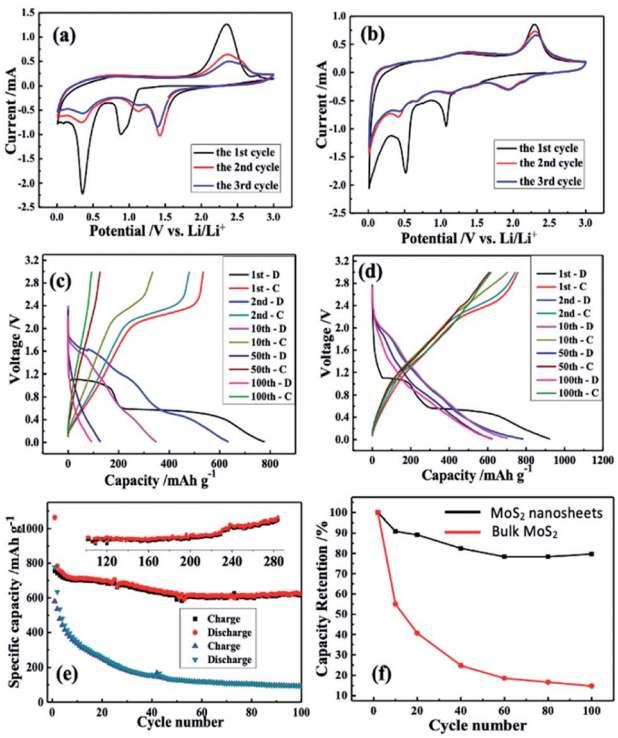

Fig. 4 Cyclic voltammograms of (a) bulk MoS_2 and (b) MoS_2 nanosheets; typical charge and discharge curves at selected cycles of (c) bulk MoS_2 and (d) MoS_2 nanosheets; (e) a comparison of the cyclic performance of bulk MoS_2 (to 100 cycles) and MoS_2 nanosheets (over 280 cycles) and (f) capacity retention *versus* cycle numbers of (i) bulk MoS_2 and (ii) MoS_2 nanosheets.

For good measure, the lithium storage behaviour of the MoS_2 anode was further measured by GCD testing *via* a CR-2032 coin. Fig. 4c and d illustrate the bulk and as-prepared charge–discharge curves of MoS_2, respectively. The first discharge curves reveal two insertion plateaus, which shift in the subsequent cycles. In the subsequent charging curve, an obvious plateau due to delithiation was noticed, which corresponds to the CV curve.

Although the charge/discharge profiles of the as-prepared MoS_2 have not considerably changed through cycling (as depicted in Fig. 4e), those of the bulk MoS_2 anode were altered after 10 cycles. In the first cycle, the bulk MoS_2 anode reported charge and discharge capacities of 581 mA h g^{-1} and 777 mA h g^{-1}, respectively, while those values of the as-prepared MoS_2 were 925 mA h g^{-1} and 657 mA h g^{-1}. It is noteworthy that the irreversible capacity in the first cycle is high, which may arise from two aspects: (1) a solid electrolyte intermediate phase (SEI) is formed on the anode surface due to the electrolyte's decomposition; (2) during the lithium insertion in MoS_2 nanosheets, lithium ions trapped in the nanoclusters or defect sites/intratubal sites cause the irreversible capacity.[23,72]

According to Fig. 4e, at a current density of 100 mA g^{-1}, the cycle performances of the bulk and the as-prepared MoS_2 are different. Noticeably, the as-prepared MoS_2 still delivers a remarkable specific energy capacity after 100 cycles, while the bulk MoS_2 anode shows an obvious capacity decay over 100 cycles. Fig. 4f displays the capacity retention of the two anodes. It is evident that the bulk MoS_2 shows a much lower capacity retention (14.8%) than the as-prepared MoS_2 (80.0%). The as-prepared MoS_2 still maintained a high capacity of 716 mA h g^{-1} in the 285th cycle (see the inset of Fig. 4e) with an average of 0.030% capacity loss per cycle, suggesting its excellent cycling performance compared with those of other MoS_2 based anode materials (Table S1†). Inclusively, the excellent cycle performance of the as-prepared MoS_2 composed of 4–8 layers is attributed to the more facilitated diffusion in the liquid

electrolyte and an increase in the electrolyte–electrode contact area compared with that of the bulk one.[73–75] Moreover, the presence of only a few layers decreases the solid-state transport length of the lithium diffusion.[70,76,77] Considering the results shown in Fig. 4, the as-prepared MoS_2 as a LIB anode can effectively enhance the battery performance to a great extent.

Conclusions

The MoS_2 nanosheets we obtained through a simple ball milling approach are only a few (4–8) layers. As an anode of LIBs, the as-prepared MoS_2 achieves an outstanding reversible capacity of 716 mA h g^{-1} after 285 cycles, which reveals an improved cyclic performance and higher energy capacity compared with those of the bulk material with a measured specific capacity of only 94 mA h g^{-1} after observation for 100 cycles. This lead to an understanding of the effect of the synthesis method on MoS_2 nanosheets for both the structural properties and the electrochemical performance. The proposed simple exfoliation process in this study can be potentially used for other layered materials, such as WS_2, SnS_2, $MoSe_2$, *etc.* Moreover, this research can be of great importance to create cost-effective ultra-thin layered anodes with a promising performance for LIB application.

Conflicts of interest

There are no conflicts to declare.

Acknowledgements

The authors gratefully acknowledge the financial support from the Natural Science Foundation of Qinghai Province of China (2020-ZJ-910), the National Natural Science Foundation of China (52072298 and 51802261), and the Natural Science Foundation of Shaanxi Province (2020JC-41).

References

1 V. Etacheri, R. Marom, R. Elazari, G. Salitra and D. Aurbach, *Energy Environ. Sci.*, 2011, **4**, 3243–3262.
2 C. Wang, C. Zhan, X. Ren, R. Lv, W. Shen, F. Kang and Z.-H. Huang, *RSC Adv.*, 2019, **9**, 42316–42323.
3 Y. Li, X. Yin, X. Huang, X. Liu and W. Wu, *Int. J. Hydrogen Energy*, 2020, **45**, 16489–16499.
4 Q. H. Wang, K. Kalantar-Zadeh, A. Kis, J. N. Coleman and M. S. Strano, *Nat. Nanotechnol.*, 2012, **7**, 699–712.
5 K.-A. N. Duerloo, Y. Li and E. J. Reed, *Nat. Commun.*, 2014, **5**, 1–9.
6 W. Zhao, J. Pan, Y. Fang, X. Che, D. Wang, K. Bu and F. Huang, *Chem.–Eur. J.*, 2018, **24**, 15942–15954.
7 L. Jiang, B. Lin, X. Li, X. Song, H. Xia, L. Li and H. Zeng, *ACS Appl. Mater. Interfaces*, 2016, **8**, 2680–2687.
8 J. R. Dahn, T. Zheng, Y. Liu and J. Xue, *Science*, 1995, **270**, 590–593.
9 T. Stephenson, Z. Li, B. Olsen and D. Mitlin, *Energy Environ. Sci.*, 2014, **7**, 209–231.
10 H. Zhao, H. Zeng, Y. Wu, S. Zhang, B. Li and Y. Huang, *J. Mater. Chem. A*, 2015, **3**, 10466–10470.
11 G. Fiori, F. Bonaccorso, G. Iannaccone, T. Palacios, D. Neumaier, A. Seabaugh, S. K. Banerjee and L. Colombo, *Nat. Nanotechnol.*, 2014, **9**, 768–779.
12 F. Xia, H. Wang, D. Xiao, M. Dubey and A. Ramasubramaniam, *Nat. Photonics*, 2014, **8**, 899–907.
13 O. V. Yazyev, *Rep. Prog. Phys.*, 2010, **73**, 056501.
14 D. Deng, K. Novoselov, Q. Fu, N. Zheng, Z. Tian and X. Bao, *Nat. Nanotechnol.*, 2016, **11**, 218–230.
15 F. Bonaccorso, L. Colombo, G. Yu, M. Stoller, V. Tozzini, A. C. Ferrari, R. S. Ruoff and V. Pellegrini, *Science*, 2015, **347**, 1246501.
16 J. Xiao, D. Choi, L. Cosimbescu, P. Koech, J. Liu and J. P. Lemmon, *Chem. Mater.*, 2010, **22**, 4522–4524.
17 J. Yuan, J. Zhu, R. Wang, Y. Deng, S. Zhang, C. Yao, Y. Li, X. Li and C. Xu, *Chem. Eng. J.*, 2020, 125592.
18 H. Tan, Y. Feng, X. Rui, Y. Yu and S. Huang, *Small Methods*, 2020, **4**, 1900563.
19 X. Man, P. Liang, H. Shu, L. Zhang, D. Wang, D. Chao, Z. Liu, X. Du, H. Wan and H. Wang, *J. Phys. Chem. C*, 2018, **122**, 24600–24608.
20 M. Remskar, A. Mrzel, Z. Skraba, A. Jesih, M. Ceh, J. Demšar, P. Stadelmann, F. Lévy and D. Mihailovic, *Science*, 2001, **292**, 479–481.
21 M. Chhowalla and G. A. Amaratunga, *Nature*, 2000, **407**, 164–167.
22 E. Pomerantseva and Y. Gogotsi, *Nat. Energy*, 2017, **2**, 1–6.
23 C. Feng, J. Ma, H. Li, R. Zeng, Z. Guo and H. Liu, *Mater. Res. Bull.*, 2009, **44**, 1811–1815.
24 Q. Su, S. Wang, M. Feng, G. Du and B. Xu, *Sci. Rep.*, 2017, **7**, 1–10.
25 J. Kong, C. Zhao, Y. Wei and X. Lu, *ACS Appl. Mater. Interfaces*, 2015, **7**, 24279–24287.
26 C. Liang, X. Sui, A. Wang, J. Chang, W. Wang, Z. Chen, W. Jiang, Y. Ma, J. Zhang and X. Liu, *Adv. Mater. Interfaces*, 2020, **7**, 2001130.
27 X. Li, J. Yang, Y. Hu, J. Wang, Y. Li, M. Cai, R. Li and X. Sun, *J. Mater. Chem.*, 2012, **22**, 18847–18853.
28 G. Cunningham, M. Lotya, C. S. Cucinotta, S. Sanvito, S. D. Bergin, R. Menzel, M. S. Shaffer and J. N. Coleman, *ACS Nano*, 2012, **6**, 3468–3480.
29 J. N. Coleman, M. Lotya, A. O'Neill, S. D. Bergin, P. J. King, U. Khan, K. Young, A. Gaucher, S. De and R. J. Smith, *Science*, 2011, **331**, 568–571.
30 H. Ramakrishna Matte, A. Gomathi, A. K. Manna, D. J. Late, R. Datta, S. K. Pati and C. Rao, *Angew. Chem., Int. Ed.*, 2010, **49**, 4059–4062.
31 Z. Zeng, Z. Yin, X. Huang, H. Li, Q. He, G. Lu, F. Boey and H. Zhang, *Angew. Chem.*, 2011, **123**, 11289–11293.
32 B. Radisavljevic, A. Radenovic, J. Brivio, V. Giacometti and A. Kis, *Nat. Nanotechnol.*, 2011, **6**, 147–150.
33 C. Lee, H. Yan, L. E. Brus, T. F. Heinz, J. Hone and S. Ryu, *ACS Nano*, 2010, **4**, 2695–2700.
34 R. Liu, D. Wu, X. Feng and K. Müllen, *J. Am. Chem. Soc.*, 2011, **133**, 15221–15223.

35 A. Ciesielski and P. Samori, *Chem. Soc. Rev.*, 2014, **43**, 381–398.
36 X. Duan, C. Wang, J. C. Shaw, R. Cheng, Y. Chen, H. Li, X. Wu, Y. Tang, Q. Zhang and A. Pan, *Nat. Nanotechnol.*, 2014, **9**, 1024–1030.
37 M.-Y. Li, Y. Shi, C.-C. Cheng, L.-S. Lu, Y.-C. Lin, H.-L. Tang, M.-L. Tsai, C.-W. Chu, K.-H. Wei and J.-H. He, *Science*, 2015, **349**, 524–528.
38 V. Nicolosi, M. Chhowalla, M. G. Kanatzidis, M. S. Strano and J. N. Coleman, *Science*, 2013, **340**, 1226419.
39 H. Liu, L. Liu, M. Yi, Z. Shen, S. Liang, X. Zhang and S. Ma, *Chem. Eng. J.*, 2017, **311**, 293–301.
40 H. Li, J. Wu, Z. Yin and H. Zhang, *Acc. Chem. Res.*, 2014, **47**, 1067–1075.
41 G. S. Bang, K. W. Nam, J. Y. Kim, J. Shin, J. W. Choi and S.-Y. Choi, *ACS Appl. Mater. Interfaces*, 2014, **6**, 7084–7089.
42 A. Jawaid, D. Nepal, K. Park, M. Jespersen, A. Qualley, P. Mirau, L. F. Drummy and R. A. Vaia, *Chem. Mater.*, 2016, **28**, 337–348.
43 A. Gupta, V. Arunachalam and S. Vasudevan, *J. Phys. Chem. Lett.*, 2016, **7**, 4884–4890.
44 X. Zhang, Z. Lai, C. Tan and H. Zhang, *Angew. Chem., Int. Ed.*, 2016, **55**, 8816–8838.
45 G. Eda, H. Yamaguchi, D. Voiry, T. Fujita, M. Chen and M. Chhowalla, *Nano Lett.*, 2011, **11**, 5111–5116.
46 D. Voiry, M. Salehi, R. Silva, T. Fujita, M. Chen, T. Asefa, V. B. Shenoy, G. Eda and M. Chhowalla, *Nano Lett.*, 2013, **13**, 6222–6227.
47 Y. H. Lee, X. Q. Zhang, W. Zhang, M. T. Chang, C. T. Lin, K. D. Chang, Y. C. Yu, J. T. W. Wang, C. S. Chang and L. J. Li, *Adv. Mater.*, 2012, **24**, 2320–2325.
48 J. Zhou, J. Lin, X. Huang, Y. Zhou, Y. Chen, J. Xia, H. Wang, Y. Xie, H. Yu and J. Lei, *Nature*, 2018, **556**, 355–359.
49 C. Han, Y. Zhang, P. Gao, S. Chen, X. Liu, Y. Mi, J. Zhang, Y. Ma, W. Jiang and J. Chang, *Nano Lett.*, 2017, **17**, 7767–7772.
50 S. Mateti, M. M. Rahman, P. Cizek and Y. Chen, *RSC Adv.*, 2020, **10**, 12754–12758.
51 F. Yang, X. Feng, P.-A. Glans and J. Guo, *APL Mater.*, 2021, **9**, 050903.
52 S. Kim, W. Park, D. Kim, J. Kang, J. Lee, H. Y. Jang, S. H. Song, B. Cho and D. Lee, *Nanomaterials*, 2020, **10**, 1045.
53 A. Tayyebi, N. Ogino, T. Hayashi and N. Komatsu, *Nanotechnology*, 2019, **31**, 075704.
54 D. He, Y. Yang, Z. Liu, J. Shao, J. Wu, S. Wang, L. Shen and N. Bao, *Nano Res.*, 2020, **13**, 1029–1034.
55 Y. Teng, H. Zhao, Z. Zhang, Z. Li, Q. Xia, Y. Zhang, L. Zhao, X. Du, Z. Du and P. Lv, *ACS Nano*, 2016, **10**, 8526–8535.
56 X. L. Li, J. P. Ge and Y. D. Li, *Chem.–Eur. J.*, 2004, **10**, 6163–6171.
57 J. I. Langford and A. Wilson, *J. Appl. Crystallogr.*, 1978, **11**, 102–113.
58 J. Wang, Z. Shen and M. Yi, *New J. Chem.*, 2020, **44**, 15887–15894.
59 G. Ke, H. Chen, J. He, X. Wu, Y. Gao, Y. Li, H. Mi, Q. Zhang, C. He and X. Ren, *Chem. Eng. J.*, 2021, **403**, 126251.
60 Y. Zhan, Z. Liu, S. Najmaei, P. M. Ajayan and J. Lou, *Small*, 2012, **8**, 966–971.
61 V. Koroteev, L. Bulusheva, A. Okotrub, N. Yudanov and D. Vyalikh, *Phys. Status Solidi B*, 2011, **248**, 2740–2743.
62 F. Chen, D. Shi, M. Yang, H. Jiang, Y. Shao, S. Wang, B. Zhang, J. Shen, Y. Wu and X. Hao, *Adv. Funct. Mater.*, 2020, 2007132.
63 Z. Deng, H. Jiang, Y. Hu, Y. Liu, L. Zhang, H. Liu and C. Li, *Adv. Mater.*, 2017, **29**, 1603020.
64 A. Zak, Y. Feldman, V. Lyakhovitskaya, G. Leitus, R. Popovitz-Biro, E. Wachtel, H. Cohen, S. Reich and R. Tenne, *J. Am. Chem. Soc.*, 2002, **124**, 4747–4758.
65 C. M. Zelenski and P. K. Dorhout, *J. Am. Chem. Soc.*, 1998, **120**, 734–742.
66 W. Zhao, M. Fang, F. Wu, H. Wu, L. Wang and G. Chen, *J. Mater. Chem.*, 2010, **20**, 5817–5819.
67 J. B. Cook, H. S. Kim, Y. Yan, J. S. Ko, S. Robbennolt, B. Dunn and S. H. Tolbert, *Adv. Energy Mater.*, 2016, **6**, 1501937.
68 R. Zhao, Y. Han, W. Li, J. Li, M. Chen and L. Chen, *Chem. Commun.*, 2020, **56**, 3007–3010.
69 Q. Wang and J. Li, *J. Phys. Chem. C*, 2007, **111**, 1675–1682.
70 X. Fang, X. Yu, S. Liao, Y. Shi, Y.-S. Hu, Z. Wang, G. D. Stucky and L. Chen, *Microporous Mesoporous Mater.*, 2012, **151**, 418–423.
71 C. Chen, X. Xie, B. Anasori, A. Sarycheva, T. Makaryan, M. Zhao, P. Urbankowski, L. Miao, J. Jiang and Y. Gogotsi, *Angew. Chem., Int. Ed.*, 2018, **57**, 1846–1850.
72 J. Li, S. Du, H. Tao and X. Yang, *Ionics*, 2020, 1–10.
73 X. Cao, C. Tan, X. Zhang, W. Zhao and H. Zhang, *Adv. Mater.*, 2016, **28**, 6167–6196.
74 Z. Li, N. Liu, X. Wang, C. Wang, Y. Qi and L. Yin, *J. Mater. Chem.*, 2012, **22**, 16640–16648.
75 C. Yuan, L. Yang, L. Hou, L. Shen, X. Zhang and X. W. D. Lou, *Energy Environ. Sci.*, 2012, **5**, 7883–7887.
76 A. Pan, J.-G. Zhang, G. Cao, S. Liang, C. Wang, Z. Nie, B. W. Arey, W. Xu, D. Liu and J. Xiao, *J. Mater. Chem.*, 2011, **21**, 10077–10084.
77 L. Li, X. Yin, S. Liu, Y. Wang, L. Chen and T. Wang, *Electrochem. Commun.*, 2010, **12**, 1383–1386.